Supplementary Information: Surface enhanced spectroscopies of a molecular monolayer in an all-dielectric nanoantenna

Javier Cambiasso,[*,†] Matthias König,[‡] Emiliano Cortés,[†] Sebastian Schlücker,[*,‡] and Stefan A. Maier[*,†,¶]

†*Blackett Laboratories, Imperial College London, Prince Consort Road, London, SW7 2BB*

‡*Physical Chemistry I, Department of Chemistry and Center for Nanointegration Duisburg-Essen (CENIDE), University of Duisburg-Essen, Universitätsstrasse 5, 45141 Essen, Germany*

¶*Chair for Hybrid Nanosystems, Faculty of Physics, Ludwig-Maximilians-Universität München, München, Germany*

E-mail: j.cambiasso@imperial.ac.uk; sebastian.schluecker@uni-due.de; s.maier@imperial.ac.uk

Contents

1 Molecular functionalization of Si nanoantennas with β-carotenal

The homogeneous molecular functionalization of Si nanoantennas with trans-β-Apo-8'-carotenal (β-carotenal) was achieved by a silane anchor (APTMS, (3-Aminopropyl)trimethoxysilane).

Briefly, β-carotenal was reacted with APTMS to form the corresponding Schiff base. The conjugate was added to the substrate containing the Si nanoantennas. The fluorescence image excited at 488 nm in figure S1(a) left shows the enhanced fluorescence from β-carotenal on the Si nanoantennas (arrays of bright spots). In addition to the Si nanoantennas also the underlying sapphire substrate was functionalized. The fluorescence brightness of the functionalized substrate in figure S1(a) left is higher than that of an unfunctionalized substrate in figure S1(a) right. A quantitative comparison of the rectangular regions in figure S1(a) was performed by averaging the fluorescence intensities along the y-direction and plotting these average values as a function of the x-coordinate. The significantly increased fluorescence from the functionalized sample (blue curve) compared to the non-functionalized sample (green curve) is obvious. The high signal level observed from the unfunctionalized sample is due to autofluorescence from the sapphire substrate at 488 nm excitation.

An additional positive control experiment was performed in order to demonstrate that the silane anchor binds to both silicon and sapphire. A sapphire substrate with silicon microstructures was first functionalized with APTMS and then incubated with citrate-stabilized AuNP for electrostatic binding[1] (figure S2(a)-(c)). The SEM images in S2(b) and (c) clearly show that the AuNP bind homogeneously to both the sapphire and the Si nanoantenna. The negative control in figure S2(d) without APTMS functionalization does not indicate the binding of AuNP. As can be seen from the SEM image in Figure S2(e), the coverage of the nanoparticles is highly homogeneous all over the surface (upper-half Si and lower-half

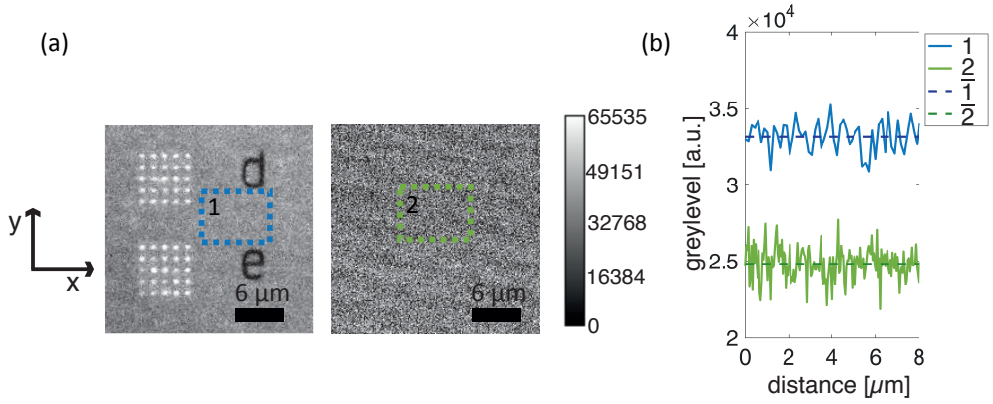

Figure S1: a) Fluorescence images of functionalized (left) and unfunctionalized (right) sample. The two boxes are highlighting the areas of the greylevel plot in (b). b) Averaged greylevel intensity of y-direction in dependance on x-direction with calculated mean value of both measurements.

sapphire). Moreover, the amount of nanoparticles tracked in a given area over both surfaces account for the same number of nanoparticles. This fact reflects that the number of surface groups able to anchor a nanoparticle are the same over both surfaces (i.e. equal surface coverage).

2 Derivation of eq. 4

For a general situation we can define the intrinsic radiation efficiency $q_0(\lambda_{\mathrm{Em}})$ as:[2–5]

$$q_0(\lambda_{\mathrm{Em}}) \stackrel{\mathrm{def}}{=} \frac{\gamma_{\mathrm{r}}^0(\lambda_{\mathrm{Em}})}{\gamma_{\mathrm{r}}^0(\lambda_{\mathrm{Em}}) + \gamma_{\mathrm{nr}}^0(\lambda_{\mathrm{Em}})}, \tag{S1}$$

where $\gamma_{\mathrm{r}}^0(\lambda_{\mathrm{Em}})$ is given by the emission of a radiating dipole in free-space:[2,6–8]

$$\gamma_{\mathrm{r}}^0(\lambda_{\mathrm{Em}}) = \frac{\|\mathbf{d}_{\mathrm{Em}}\|^2}{3\pi\varepsilon_0\hbar c^3} \overbrace{\left(\frac{2\pi c}{\lambda_{\mathrm{Em}}}\right)^3}^{\omega_{\mathrm{Em}}^3}, \tag{S2}$$

with $\mathbf{d}_{\mathrm{Em}}$ the transition dipole moment of the molecule from the radiative energy level to the ground state, ε_0 the free-space permittivity, $\hbar$ the reduced Planck's constant, c the speed of

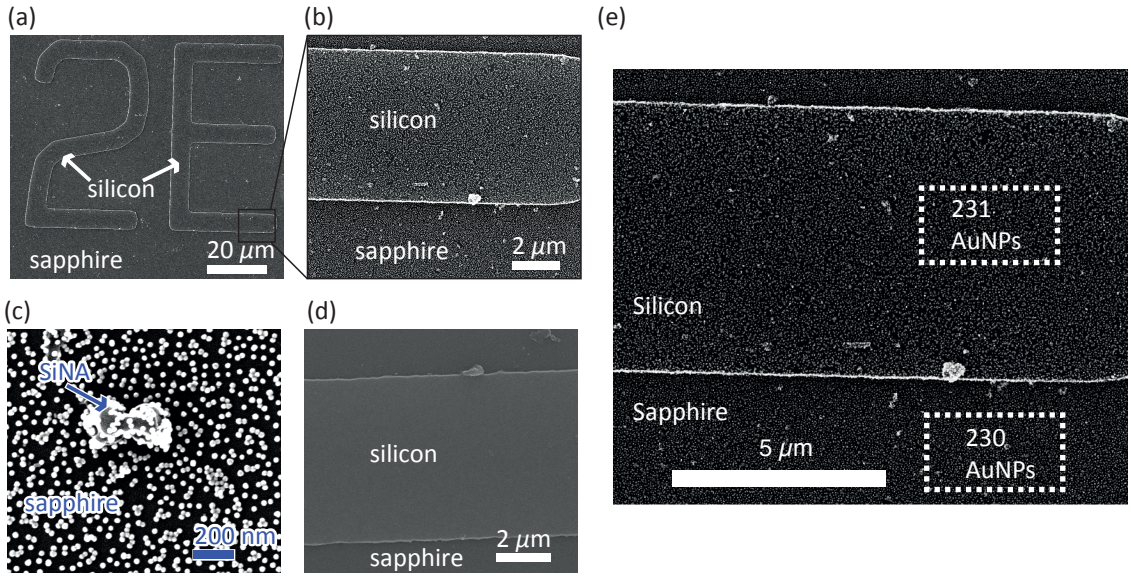

Figure S2: SEM images of APTMS functionalized sample (a)-(c) and negative control sample (d) (unfunctionalized), which was dipped into a gold colloid ($d = 26\,nm$, $[AuNP] = 400\,pM$) for 24 h. Afterwards the sample was rinsed with water to remove unbound particles. (e) Zoom of (b) showing the homogeneity of the AuNP surface coverage. Rectangles (dotted white) in both images have the same dimensions ($1.00\ \mu m \times 0.55\ \mu m$) and the number of 26 nm AuNP found in each of them are 231 for Si and 230 for sapphire. These results point that the APTMS surface coverage can be estimated to be the same for both surfaces. To enhance the contrast in SEM measurements a 3 nm Pt layer was sputtered onto the sample.

light in vacuum and λ_{Em} the wavelength associated with the transition. Similarly, $\gamma_{\mathrm{nr}}^{0}(\lambda_{\mathrm{Em}})$ is the rate of decay into non-radiative channels that takes into account the coupling to internal degrees of freedom. The non-radiative decay rate can be cast in the form of:

$$\frac{\gamma_{\mathrm{nr}}^{0}(\lambda_{\mathrm{Em}})}{\gamma_{\mathrm{r}}^{0}(\lambda_{\mathrm{Em}})} = \frac{1 - q_0(\lambda_{\mathrm{Em}})}{q_0(\lambda_{\mathrm{Em}})}, \tag{S3}$$

where the right hand side measures the non-radiative rate relative to the free-space radiation.

Contrarily, when an emitter is placed in closed proximity to an object that modifies the local density of optical states,[2,9–12] like an optical nanoantenna, it will effectively see new decay mechanisms which can be identified as radiative and non-radiative. The former modify the rate $\gamma_{\mathrm{r}}(\lambda_{\mathrm{Em}})$ at which the emitter couples to the detectable far-field, while the latter modifies the rate $\gamma_{\mathrm{nr}}(\lambda_{\mathrm{Em}})$ at which it can couple to near field modes. It is thus necessary to redefine the radiation efficiency of an emitter in the vicinity of an antenna to take account this new decay channels:[2,4,12]

$$q(\lambda_{\mathrm{Em}}) \stackrel{\mathrm{def}}{=} \frac{\gamma_{\mathrm{r}}(\lambda_{\mathrm{Em}})}{\gamma_{\mathrm{r}}(\lambda_{\mathrm{Em}}) + \gamma_{\mathrm{nr}}(\lambda_{\mathrm{Em}}) + \gamma_{\mathrm{nr}}^{0}(\lambda_{\mathrm{Em}})}. \tag{S4}$$

Here it was assumed that the interaction of the molecule with light does not modify the intrinsic non-radiative channels. With equation S3 we can express this parameter in terms of both simulated and phenomenological values as follows:[2,13]

$$q(\lambda_{\mathrm{Em}}) = \frac{\gamma_{\mathrm{r}}(\lambda_{\mathrm{Em}})/\gamma_{\mathrm{r}}^{0}(\lambda_{\mathrm{Em}})}{\Gamma(\lambda_{\mathrm{Em}}) + \frac{1-q_0(\lambda_{\mathrm{Em}})}{q_0(\lambda_{\mathrm{Em}})}}, \tag{S5}$$

where $\gamma_{\mathrm{r}}^{0}(\lambda_{\mathrm{Em}})/\gamma_{\mathrm{r}}^{0}(\lambda_{\mathrm{Em}})$ is the radiative rate enhancement compared to its value in vacuum for a single photon emitter with unity radiation efficiency and

$$\begin{aligned} \Gamma(\lambda_{\mathrm{Em}}) =& \frac{\gamma_{\mathrm{r}}(\lambda_{\mathrm{Em}}) + \gamma_{\mathrm{nr}}(\lambda_{\mathrm{Em}})}{\gamma_{\mathrm{r}}^{0}} \\ =& \frac{\gamma_{\mathrm{tot}}(\lambda_{\mathrm{Em}})}{\gamma_{\mathrm{r}}^{0}(\lambda_{\mathrm{Em}})} \end{aligned} \tag{S6}$$

is the ratio of total decay rate to vacuum decay rate, again for a single photon emitter with unity quantum efficiency. $\Gamma(\lambda_{\mathrm{Em}})$ is also known as the Purcell enhancement factor[14–16] for unity intrinsic yield emitters. All these parameters are easily accessible from classical simulations and allow us to compute the fluorescence enhancement:

$$\mathcal{F} \sim \overbrace{|\mathbf{d}\cdot\mathbf{E}|^2}^{\text{Excitation enhancement}} \times \overbrace{q}^{\text{Radiation efficiency}}. \tag{S7}$$

by using equation S5.

Notwithstanding, care must be taken to theoretically compute these values and compare them with the experimentally measured data. More specifically, the radiative rate enhancement $\gamma_{\mathrm{r}}(\lambda_{\mathrm{Em}})/\gamma_{\mathrm{r}}^{0}(\lambda_{\mathrm{Em}})$ must be obtained by taking into account the numerical aperture of the experimental setup to properly describe the experimentally obtainable quantities.

3 Behaviour an emitter close to a substrate

In order to understand the origin of the large SERS and SEF enhancements in dielectric structures we propose to compare the factors obtained by comparing the Raman and fluorescence enhancements relative to vacuum and not relative to the molecule on the sapphire substrate. It must be emphasized that the simulated enhancement factors took into account the effect of the substrate on the emitter. The reference values in the text were those of emitters on sapphire and not of those of emitters in vacuum.

In particular the SERS enhancement factor when comparing with the behavior in vacuum ($\emptyset$) is given by:

$$\eta_{\mathrm{SERS}}^{\emptyset} \equiv \mathcal{R}_{\mathrm{D}}(\lambda_{\mathrm{Exc}}, \lambda_{\mathrm{R}}), \tag{S8}$$

and the corresponding enhancement factor for SEF is:

$$\eta_{\mathrm{SEF}}^{\emptyset} = \frac{\left|\mathbf{d}_{\mathrm{Exc}}\cdot\mathbf{E}(\mathbf{r}_{\mathrm{E}};\lambda_{\mathrm{Exc}})\right|^2}{\left|\mathbf{d}_{\mathrm{Exc}}\cdot\mathbf{E}_0\right|^2} \int \frac{q_{\mathrm{NA}}(\lambda_{\mathrm{Em}})}{q_0}\zeta(\lambda_{\mathrm{Exc}},\lambda_{\mathrm{Em}})\vartheta(\lambda_{\mathrm{Em}})\,\mathrm{d}\lambda_{\mathrm{Em}}, \tag{S9}$$

where $\mathbf{d}_{\mathrm{Exc}}$ is the transition dipole moment from the ground state to the excited state and $\mathbf{E}(\mathbf{r}_{\mathrm{E}};\lambda_{\mathrm{Exc}})$ is the excitation electric field at the position of the dipole obtained by solving Maxwell's equations without the dipolar emitter. Moreover, the absorption $\alpha(\lambda_{\mathrm{Exc}})$ and emission $\zeta(\lambda_{\mathrm{Exc}},\lambda_{\mathrm{Em}})$ are chosen to satisfy the normalization condition $\int \zeta(\lambda_{\mathrm{Exc}},\lambda_{\mathrm{Em}})\vartheta(\lambda_{\mathrm{Em}})\,\mathrm{d}\lambda_{\mathrm{Em}} = 1$. Here, This normalization physically implies the desired condition that the setup is tailored to detect light of some emitted wavelength with certainty. It is worth noting that the first factor is the usual field enhancement projected on the absorption transition dipole direction, and the second factor is just a spectrally averaged enhancement of radiation efficiency.

Clearly the situation where the comparison with vacuum provides the approximately correct normalization for the enhancement factors is such that the molecule is located far from the surface. For example, if the quantity of interest is being compared to one measured in a diluted solution, a comparison with a homogeneous medium can be made given that the participating molecules can be several hundreds of nanometers away from the surface. The only caveat is that the refractive index of the homogenous medium has to be taken into account in equation S9 whereby the total enhancement factor gets amplified by a factor n, with n the refractive index of the surrounding medium. Several examples of this situation can be found in literature, for example in the work by Regmi *et al.*[17] using Si dimers or in the works by Holzmeister *et al.*[18] and Kinkhabwala *et al.*[3] using metallic nanoantennas.

Another possibility is that the refractive index is close to unity. For example both the $\eta^{\emptyset}_{\mathrm{SERS}}$ and the excitation enhancement cannot appreciably change under this assumptions as can be derived below. Both quantities can be obtained by solving the total field incident on a substrate with a complex dispersive refractive index n. The solution can be expressed in terms of the Fresnel coefficients[19] and yields:

$$\frac{|\hat{\mathbf{x}}\cdot\mathbf{E}(\mathbf{r},\lambda_{\mathrm{Exc}})|^2}{|\hat{\mathbf{x}}\cdot\mathbf{E}_0|^2} = \left|1+\left[\frac{n(\lambda_{\mathrm{Exc}})-1}{n(\lambda_{\mathrm{Exc}})+1}\right]^2\right|^2, \tag{S10}$$

where the dipole moment was chosen parallel to $\hat{\mathbf{x}}$ because it is the only electric field compo-

nent that yields a non-zero excitation enhancement. Notice that excitation value is independent of the position of the emitter. For sapphire the excitation enhancement yields 0.87 and the Raman enhancement factor $0.87^2 = 0.76$. Both quantities are close to unity, indicating that if the measured excitation rate or the total Raman enhancement factor is compared to that of vacuum instead of with the dye on the substrate, the modifications should be of at most a 30%.

Figure S3(a) shows the region in the permittivity space where the excitation enhancement values are one (dashed line). We can see that SiO_2, a substrate of excellence, is close to the unity iso-curve, indicating that a comparison with vacuum would not be too deviated from the experimental situation where the enhancements are calculated relative to molecules on a surface. Furthermore, we can observe that high index materials like GaP and Si present problems with this approximation. The behavior for metals is the expected one: they enhance the Raman scattering of molecules close to their surface, as long as a local permittivity function suffices to describe their behavior.[20–23]

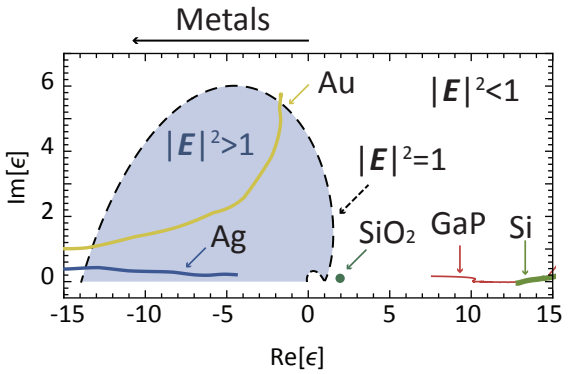

Figure S3: Region in permittivity-space where both the excitation enhancement and the Raman enhancement of a dye close to a surface are close to unity. Several materials are highlighted. The closer they are to the dashed curve, the closer the enhancement is to unity, therefore rendering it indistinguishable from the vacuum case. Inside the dashed area we obtain the expected higher than vacuum behavior. The refractive indices of Au, Ag, SiO_2 and Si were taken from Palik,[24] whereas that of GaP from Jellison *et al.*[25]

The problem with comparing the radiation of an emitter in a nanoantenna to that in vacuum in the strong modifications of the radiation efficiency when it is located close to a

substrate.[2] This values can effectively tend to zero[26,27] for materials with strong quenching, but even more importantly, in an experimental setup where the detection is from the back (*cf.* figure 3(a)), most of the experimentally attainable radiation is going to be transferred to the substrate.[2] In other words, substrates with effectively zero losses could in principle be neglected in the calculations if the radiation is measured from the substrate side to capture most of the emitted energy and if the refractive index is not too high so as to strongly modify the excitation enhancement. The role of the antenna is to provide a local density of optical states that can allow the coupling to far-field radiation in the back direction by breaking the planar symmetry. The Raman enhancement does not suffer such stark modifications, given that it only depends on the electric field and not on the local density of optical states.

4 Supporting data

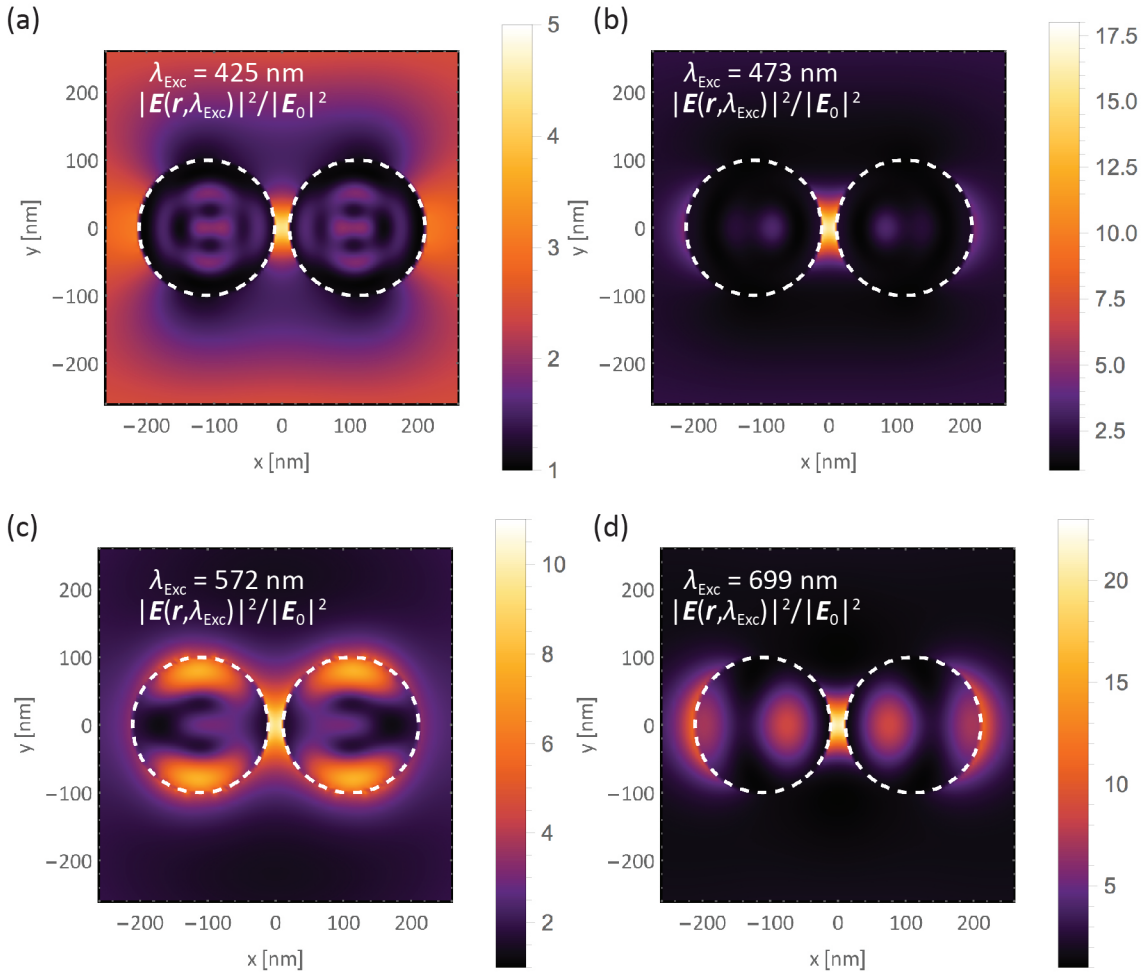

Figure S4: Near field enhancement maps at different excitation wavelengths for a Si dimer of 20 nm gap.

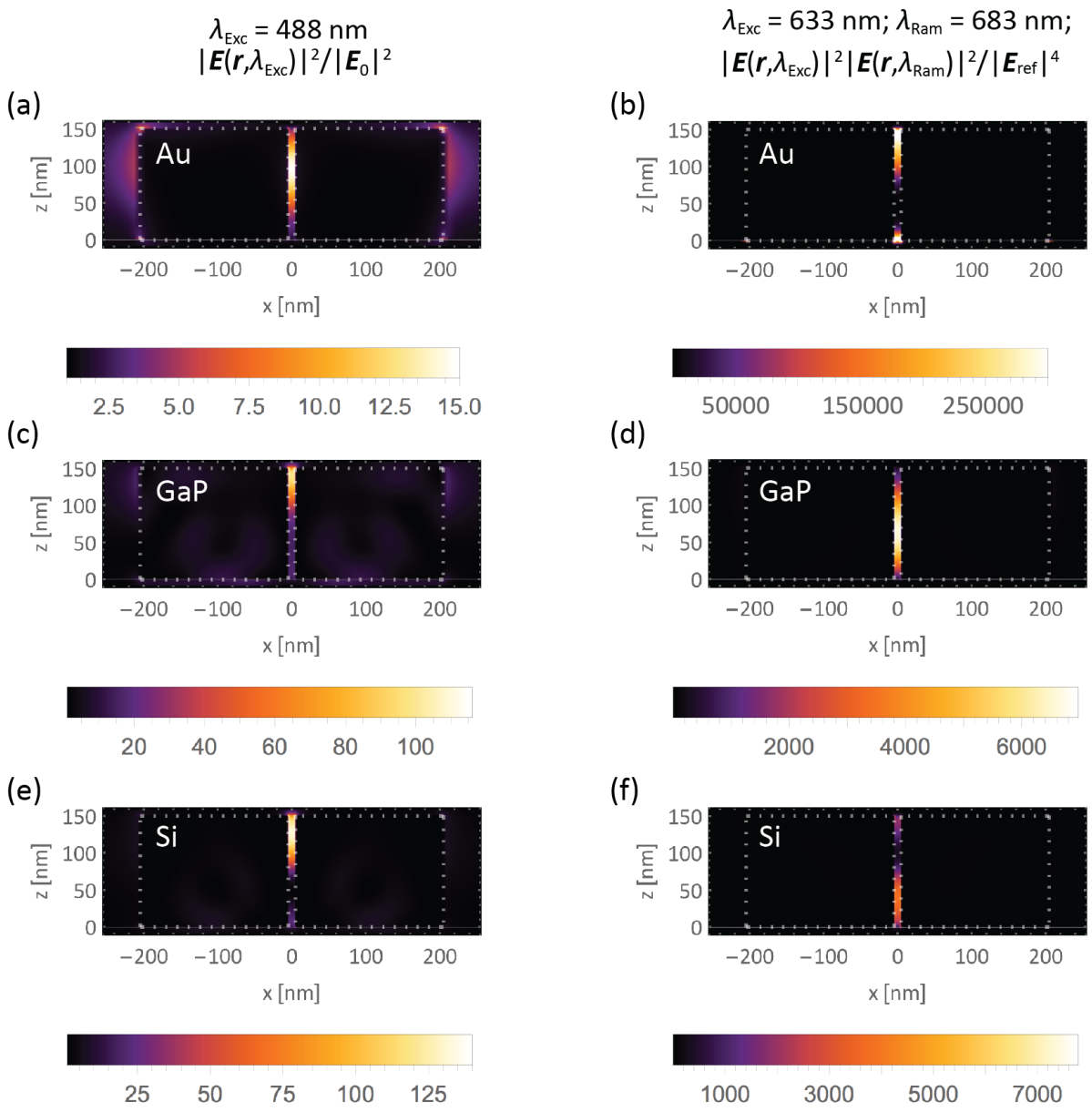

Figure S5: (a),(c),(e) Excitation enhancement maps at 488 nm excitation wavelength for a Si, GaP and Au dimer of 20 nm gap, respectively. (b),(d),(f) Raman enhancement factor maps at 633 nm excitation wavelength and $\delta\nu_1$ =1154 cm^{-1} $\Rightarrow$ 683 nm. It must be noted that even though the field enhancement of a Au nanoparticle at 488 nm (a) is much smaller than that of Si at the same wavelength due to losses, this behavior is strongly inverted in the region of high performance of Au (b) at 633 nm. Fig. S9 further supports the fact that Au nanoparticles are still suitable candidates above $\lambda = 600$ nm. Moreover, in contrast to Regmi et al.[17] the maximum field enhancement in (f) is found at the bottom of the nanostructure instead of at the top because the illumination conditions are different (from the air side in our case and from the substrate side in theirs).

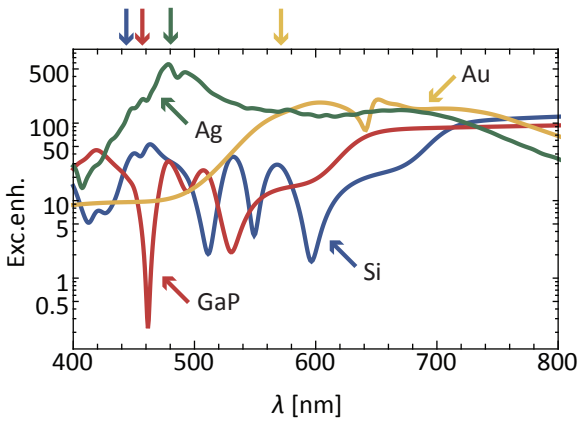

Figure S6: Excitation enhancement for Si, GaP, Au and Ag for a nanostructure of 10 nm gap, 100 nm radius and 150 nm height on top of a sapphire substrate. Notice that excitation of the emitter in the middle of the gap coincides to when it is only 1 nm away from the surface. The highlighted arrows on the top of the frame of the figure indicate the wavelength at which the simulations of fluorescence enhancement were done.

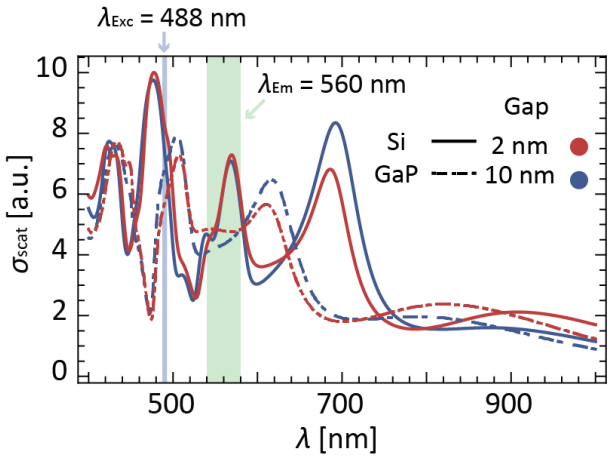

Figure S7: Scattering cross-sections for Si and GaP nanoantenna of either 10 nm or 2 nm.

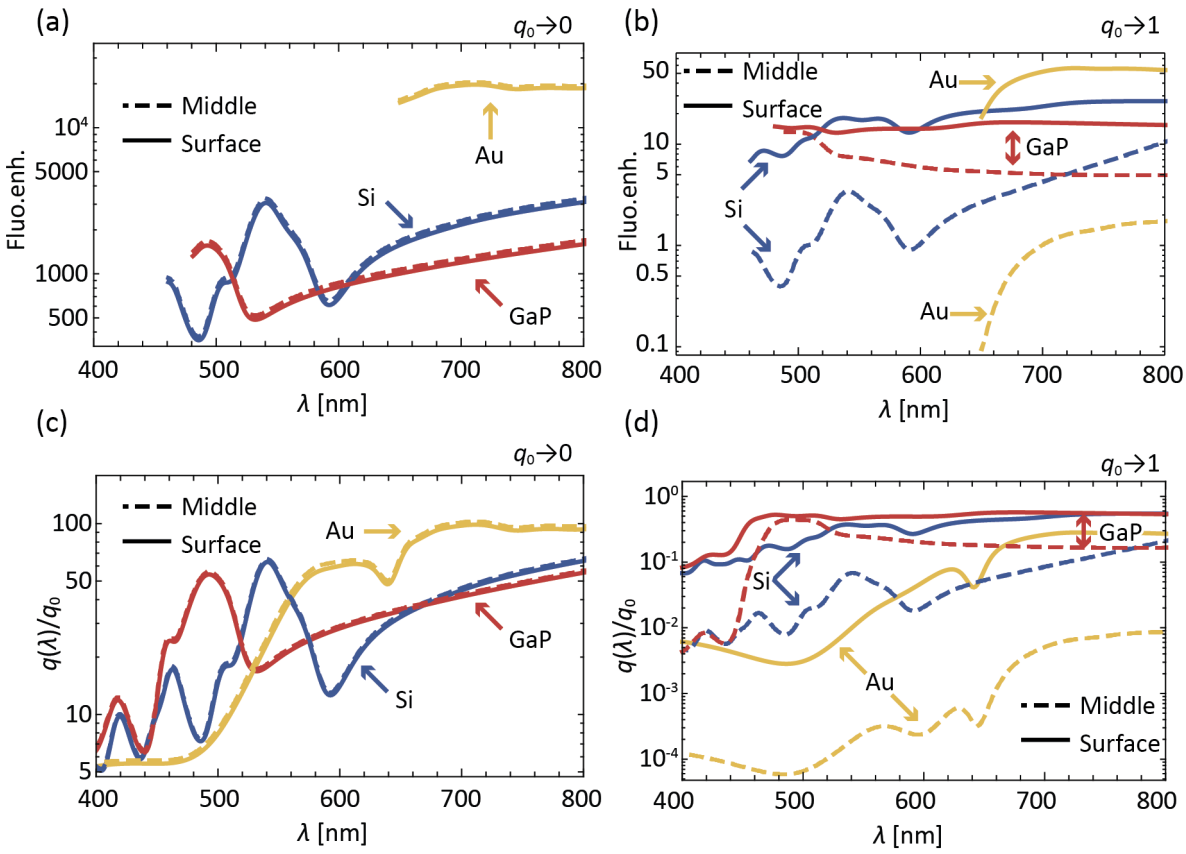

Figure S8: (a),(b) Fluorescence enhancement of an emitter in a structure of 10 nm gap either in the middle (solid lines) or in the surface (dashed lines) for Si, GaP or Au in the limits of low (a) or high quantum yield (b) at 480 nm excitation. (c),(d) Radiation efficiency of an emitter in a structure of 10 nm gap either in the middle (solid lines) or in the surface (dashed lines) for Si, GaP or Au in the limits of low (c) or high quantum yield (d).

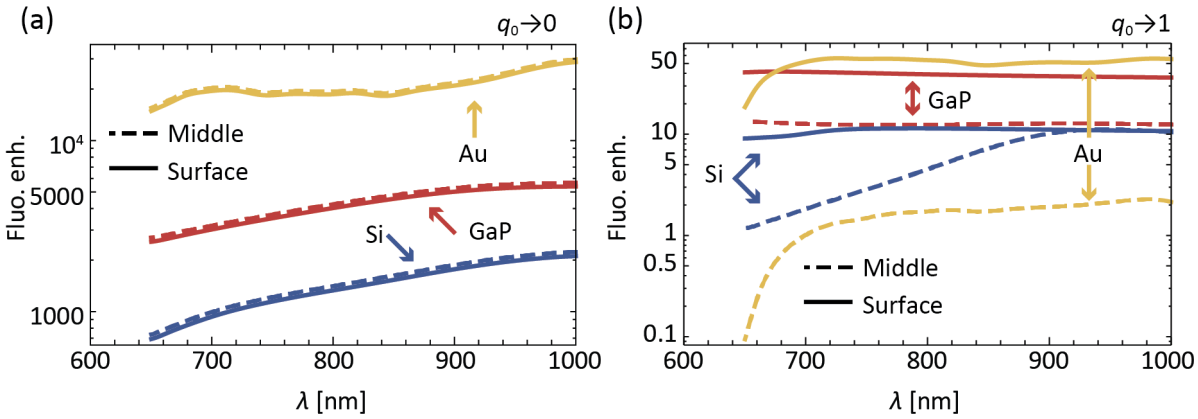

Figure S9: (a),(b) Fluorescence enhancement of an emitter in a structure of 10 nm gap either in the middle (solid lines) or in the surface (dashed lines) for Si, GaP or Au in the limits of low (a) or high quantum yield (b). In contrast to figure S8, the excitation is taken to be at $\lambda_{\mathrm{Exc}} = 650$ nm for all the structures.

References

(1) Cha, H.; Yoon, J. H.; Yoon, S. Probing quantum plasmon coupling using gold nanoparticle dimers with tunable interparticle distances down to the subnanometer range. *ACS Nano* **2014**, *8*, 8554–8563.

(2) Novotny, L.; Hecht, B. *Principles of Nano-Optics*, 2nd ed.; Cambridge, 2012.

(3) Kinkhabwala, A.; Yu, Z.; Fan, S.; Avlasevich, Y.; Müllen, K.; Moerner, W. Large single-molecule fluorescence enhancements produced by a bowtie nanoantenna. *Nat. Photon.* **2009**, *3*, 654–657.

(4) Giannini, V.; Sánchez-Gil, J. A.; Muskens, O. L.; Rivas, J. G. Electrodynamic calculations of spontaneous emission coupled to metal nanostructures of arbitrary shape: nanoantenna-enhanced fluorescence. *JOSA B* **2009**, *26*, 1569–1577.

(5) Mack, D. L.; Cortés, E.; Giannini, V.; Török, P.; Roschuk, T.; Maier, S. A. Decoupling absorption and emission processes in super-resolution localization of emitters in a plasmonic hotspot. *Nat. Commun.* **2017**, *8*, 14513.

(6) Tai, C.-t. *Dyadic green functions in electromagnetic theory*, 2nd ed.; IEEE Press: Piscataway, NJ, 1994.

(7) Jackson, J. D. *Classical Electrodynamics*, 3rd ed.; John Wiley & Sons, Inc., 1999.

(8) Devaney, A. J. *Mathematical foundations of imaging, tomography and wavefield inversion*; Cambridge Univ Press, 2012.

(9) Mandel, L.; Wolf, E. *Optical coherence and quantum optics*; Cambridge University Press: Cambridge, 1995.

(10) Milonni, P. W. *The quantum vacuum: an introduction to quantum electrodynamics*; Academic Press: Boston, 1994.

(11) Novotny, L.; van Hulst, N. Antennas for light. *Nat. Photon.* **2011**, *5*, 83–90.

(12) Giannini, V.; Fernández-Domínguez, A. I.; Heck, S. C.; Maier, S. A. Plasmonic nanoantennas: fundamentals and their use in controlling the radiative properties of nanoemitters. *Chem. Rev.* **2011**, *111*, 3888–3912.

(13) Klimov, V. I. Spectral and dynamical properties of multiexcitons in semiconductor nanocrystals. *Annu. Rev. Phys. Chem.* **2007**, *58*, 635–73.

(14) Koenderink, A. F. On the use of Purcell factors for plasmon antennas. *Opt. Lett.* **2010**, *35*, 4208–4210.

(15) Lounis, B.; Orrit, M. Single-photon sources. *Reports on Progress in Physics* **2005**, *68*, 1129.

(16) Purcell, E. M.; Torrey, H. C.; Pound, R. V. Resonance Absorption by Nuclear Magnetic Moments in a Solid. *Phys. Rev.* **1946**, *69*, 37–38.

(17) Regmi, R.; Berthelot, J.; Winkler, P. M.; Mivelle, M.; Proust, J.; Bedu, F.; Ozerov, I.; Begou, T.; Lumeau, J.; Rigneault, H.; García-Parajó, M. F.; Bidault, S.; Wenger, J.;

Bonod, N. All-Dielectric Silicon Nanogap Antennas To Enhance the Fluorescence of Single Molecules. *Nano Lett.* **2016**, *16*, 5143–51.

(18) Holzmeister, P.; Pibiri, E.; Schmied, J. J.; Sen, T.; Acuna, G. P.; Tinnefeld, P. Quantum yield and excitation rate of single molecules close to metallic nanostructures. *Nat. Commun.* **2014**, *5*, 5356.

(19) Born, M.; Wolf, E. *Principles of optics: electromagnetic theory of propagation, interference and diffraction of light*, 7th ed.; Cambridge University Press: Cambridge, 1999.

(20) Bruus, H.; Flensberg, K. *Many-body quantum theory in condensed matter physics: an introduction*; Oxford University Press: Oxford, 2004.

(21) Khurgin, J. B.; Boltasseva, A. Reflecting upon the losses in plasmonics and metamaterials. *MRS Bulletin* **2012**, *37*, 768–779.

(22) Khurgin, J. B. How to deal with the loss in plasmonics and metamaterials. *Nat. Nanotech.* **2015**, *10*, 2–6.

(23) Raza, S.; Bozhevolnyi, S. I.; Wubs, M.; Mortensen, N. A. Nonlocal optical response in metallic nanostructures. *Journal of Physics: Condensed Matter* **2015**, *27*, 183204.

(24) Palik, E. D.; Ghosh, G. *Handbook of optical constants of solids*; Academic Press: San Diego, 1998.

(25) Jellison, G. E. Optical functions of GaAs, GaP, and Ge determined by two-channel polarization modulation ellipsometry. *Opt. Mater.* **1992**, *1*, 151–160.

(26) Anger, P.; Bharadwaj, P.; Novotny, L. Enhancement and quenching of single-molecule fluorescence. *Phys. Rev. Lett.* **2006**, *96*, 113002.

(27) Manfrinato, V. R.; Wanger, D. D.; Strasfeld, D. B.; Han, H.-S.; Marsili, F.; Arrieta, J. P.; Mentzel, T. S.; Bawendi, M. G.; Berggren, K. K. Controlled placement of colloidal quantum dots in sub-15 nm clusters. *Nanotechnology* **2013**, *24*, 125302.